# Matching Pursuit-Based Sliced Wigner Higher Order Spectral Analysis for Seismic Signals

Yuqing Wang, Zhenming Peng, *Member, IEEE*, Xiaoyang Wang, and Yanmin He

***Abstract*—The Wigner higher order spectra (WHOS) are multidimensional time–frequency distributions defined by extending the Wigner–Ville distribution (WVD) to higher order spectra domains. As a subset of WHOS, the sliced WHOS (SWHOS) are used for conveniently representing time–frequency spectra. The SWHOS provide a better localized time–frequency support compared with WVD, but still suffers from cross term issues. Therefore, we propose a matching pursuit-based sliced Wigner higher order spectra (MP-SWHOS) algorithm, which can obtain a sparser high-resolution time–frequency spectrum without cross terms. The performance of MP-SWHOS is assessed on a simulated model and real data. The application to seismic spectral decomposition shows that the proposed algorithm can provide single-frequency slices with greater precision, important in the analysis of hydrocarbon reservoirs.**

***Index Terms*—Constant-phase Ricker wavelet, matching pursuit (MP), seismic signal, sliced Wigner higher order spectra (SWHOS), spectral decomposition.**

## I. Introduction

SPECTRAL decomposition, transforming seismic traces into the time–frequency domain, is a technique useful for analyzing seismic data to reveal information about hydrocarbon reservoirs. Different time–frequency analysis methods are able to influence the performance of spectral decomposition. Some well-known time–frequency analysis methods including short-time Fourier transform (STFT), S transform, continuous-wavelet transform, and Wigner–Ville distribution (WVD) suffer from various deficiencies. The STFT, for instance, is unable to simultaneously provide both good time resolution and good frequency resolution. This is due to the window function applied to the Fourier transform, which is limited by the Heisenberg uncertainty principle. In addition, as nonlinear time–frequency analysis, WVD can obtain the energy distribution with high time–frequency resolution, but perform poorly for multicomponent signals. There are serious cross terms in the analysis of multicomponent signals. Recently, efforts have been made to solve the cross term issue of WVD [1]–[6] and develop new time–frequency analysis methods for seismic exploration [7]–[12].

The matching pursuit (MP) proposed by Mallat and Zhang [13] is a flexible and adaptive signal decomposition algorithm. It decomposes any signal into a linear expansion of atoms that can best match the signal structures. These atoms belong to a redundant dictionary that is constructed according to prior information about the signal. Every atom is monocomponent so that its WVD does not exhibit cross term phenomenon. The sum total of all WVD results is regarded as the MP time–frequency spectrum (MP plus WVD is referred as MP-WVD). Therefore, the MP time–frequency spectrum does not suffer from the cross term problem and has a high time–frequency resolution. The MP method has been applied in various research fields [14]–[16], including seismic signal analysis [17]–[22]. Chakraborty and Okaya [17] applied MP to seismic spectral decomposition and achieved good results. Liu *et al.* [18], [19] introduced the Ricker wavelet and the Morlet wavelet to construct a dictionary for the MP method and used them for seismic spectral decomposition. Wang [20] showed a complete MP decomposition method based on complex-trace optimal search to improve efficiency. Zhao and Song [21] expanded the dictionary to be the collection of Ricker, Morlet, and mixed phase seismic wavelets. Lin *et al.* [22] combined the MP algorithm and time–frequency peak filtering to apply to random noise attenuation and seismic signal enhancement.

Higher order spectra are known as the spectral representation of higher order correlations with significant properties. Efforts have been made to develop the Wigner higher order spectra (WHOS) by extending WVD into the higher order spectra domains [23]–[28]. The WHOS are regarded as a general class of higher order time–frequency representations in the multifrequency space. A higher order WHOS will lead to a large increase in the computational complexity. For conveniently representing and computing, the sliced WHOS (SWHOS) were proposed by taking one two-dimensional slice in the multifrequency space. Its most important characteristic is the ability to represent the higher order correlation in the time–frequency spectrum. However, SWHOS also have some disadvantages that limit the application development. Cross term interference arises in the time–frequency spectrum of SWHOS. In addition, SWHOS have the computational complexity problem.

In this paper, we propose the matching pursuit-based sliced Wigner higher order spectra (MP-SWHOS) method. This approach can effectively solve the cross term problem and obtain

Manuscript received January 27, 2017; revised March 7, 2017; accepted April 15, 2017. Date of publication May 7, 2017; date of current version August 9, 2017. This work is supported by the National Natural Science Foundation of China under Grant 61571096, Grant 41274127, Grant 41301460, and Grant 40874066. *(Corresponding author: Zhenming Peng.)*

Y. Wang, Z. Peng, X. Wang, and Y. He are with the School of Optoelectronic Information and the Center for Information Geoscience, University of Electronic Science and Technology of China, Chengdu 610054, China (e-mail: wangyuqing@hotmail.com; zmpeng@uestc.edu.cn; 522657485@qq.com; heyanmin@uestc.edu.cn).

Color versions of one or more of the figures in this paper are available online at http://ieeexplore.ieee.org.

Digital Object Identifier 10.1109/JSTARS.2017.2696879

the sparser time–frequency spectrum with higher concentration than MP-WVD. The computational efficiency of MP-SWHOS is discussed in detail. The performance of the proposed method is illustrated by experiments on both simulated and real seismic data. We also apply the MP-SWHOS into the seismic spectral decomposition to verify the effectiveness.

## II. Proposed Method

### A. The Review of Matching Pursuit

Regarding the characteristics of seismic data, the Ricker wavelet with constant-phase correction is considered to be the atom for MP decomposition in this paper. A constant-phase Ricker wavelet $g_\gamma(t) = w(t)\cdot\cos(\varphi) - \mathrm{H}[w(t)]\cdot\sin(\varphi)$ related to $w(t) = (1-2(\pi f(t-u))^2)e^{-(\pi f(t-u))^2}$ [29] can be characterized by the parameter set $\gamma = \{u, f, \varphi\}$, where $\mathrm{H}[\cdot]$ denotes Hilbert transform, $u$ is the time delay, $f$ is the dominant frequency, and $\varphi$ is the phase modulation. Hence, a redundant constant-phase Ricker wavelet dictionary $D$ can be constructed by exploiting these three parameters.

The MP algorithm decomposes signal into a linear combination of atoms. After $N$ iterations, a real signal $x(t)$ can be written as

$$x(t) = \sum_{n=0}^{N-1} a_n g_{\gamma_n}(t) + R^N\{x(t)\} \tag{1}$$

where $a_n = |\langle R^n\{x(t)\}, g_{\gamma_n}(t)\rangle|$ represents the amplitude of atom $g_{\gamma_n}(t)$ ($\langle\cdot\rangle$ denotes the inner product), $g_{\gamma_n}(t)$ is the $n$th best match atom with the parameter set $\gamma_n = \{u_n, f_n, \varphi_n\}$, and $R^n\{x(t)\}$ is the $n$th residual with $R^0\{x(t)\} = x(t)$. Moreover, $R^n\{x(t)\}$ is the signal to be decomposed in the $(n+1)$th iteration.

The $n$th best match atom $g_{\gamma_n}(t)$ can be calculated by

$$g_{\gamma_n}(t) = \arg\max_{g_\gamma \in D} |\langle R^n\{x(t)\}, g_\gamma(t)\rangle| \tag{2}$$

where $D$ denotes dictionary.

When $n$ reaches at the given value $N-1$, the decomposition process is finished and $R^n\{x(t)\}$ is considered as noise interference. Then, the reconstructed signal $\hat{x}(t)$ can be given by

$$\hat{x}(t) = \sum_{n=0}^{N-1} a_n g_{\gamma_n}(t) \tag{3}$$

and its corresponding time–frequency spectrum is defined as [13]

$$\mathrm{MP-WVD}(t,f) = \sum_{n=0}^{N-1} {a_n}^2 W_{g_{\gamma_n}}(t,f) \tag{4}$$

where $W_{g_{\gamma_n}}(t,f)$ stands for the WVD of $g_{\gamma_n}(t)$, that is,

$$W_{g_{\gamma_n}}(t,f) = \int_\tau g^*_{\gamma_n}\left(t-\frac{\tau}{2}\right)\cdot g_{\gamma_n}\left(t+\frac{\tau}{2}\right)\cdot e^{-j2\pi f\tau}d\tau \tag{5}$$

### B. The Review of Sliced Wigner Higher Order Spectra

The WHOS of order $k$ of signal $x(t)$ is defined as

$$W_{kx}(t,f_1,\ldots,f_k) = \int_{\tau_1}\cdots\int_{\tau_k} r_{kt}(\tau_1,\tau_2,\ldots,\tau_k)\cdot\prod_{i=1}^{k} e^{-j2\pi f_i\tau_i}d\tau_i \tag{6}$$

where $r_{kt}(\tau_1,\tau_2,\ldots,\tau_k)$ represents the $k$th order local correlation function with expression

$$r_{kt}(\tau_1,\tau_2,\ldots,\tau_k) = x^*\left(t-\frac{1}{k+1}\sum_{m=1}^{k}\tau_m\right)\cdot\prod_{i=1}^{k} x\left(t+\frac{k}{k+1}\tau_i-\frac{1}{k+1}\sum_{j=1,j\neq i}^{k}\tau_j\right) \tag{7}$$

From (6), it is clear that the $k$th order WHOS is a function of $k+1$ variables, whose resulting plot is difficult to display. In addition, the computational complexity of WHOS is $\mathrm{O}(N^{k+1}\log_2 N)$ ($N$ represents the total number of signals), demanding for a huge time cost. Therefore, we select a two-dimensional slice of Wigner bispectrum and trispectrum to represent the time–frequency distributions in terms of instantaneous higher order moments of the signal.

The sliced Wigner bispectrum (SWB) for $k=2$ [23]–[26]

$$\begin{aligned} SW_{2x}(t,f) &= W_{2x}(t,f_1,f_2)|_{f_1=f_2=f} \\ &= \int_{\tau_1}\int_{\tau_2} x^*\left(t-\frac{1}{3}\tau_1-\frac{1}{3}\tau_2\right)\cdot x\left(t+\frac{2}{3}\tau_1-\frac{1}{3}\tau_2\right) \\ &\quad\cdot x\left(t+\frac{2}{3}\tau_2-\frac{1}{3}\tau_1\right)\cdot e^{-j2\pi f(\tau_1+\tau_2)}d\tau_1 d\tau_2 \end{aligned} \tag{8}$$

the sliced Wigner trispectrum (SWT) for $k=3$

$$\begin{aligned} SW_{3x}(t,f) &= W_{3x}(t,f_1,f_2,f_3)|_{f_1=f_2=-f_3=f} \\ &= \int_{\tau_1}\int_{\tau_2}\int_{\tau_3} x^*\left(t-\frac{1}{4}\tau_1-\frac{1}{4}\tau_2-\frac{1}{4}\tau_3\right) \\ &\quad\cdot x\left(t+\frac{3}{4}\tau_1-\frac{1}{4}\tau_2-\frac{1}{4}\tau_3\right)\cdot x\left(t+\frac{3}{4}\tau_2-\frac{1}{4}\tau_1-\frac{1}{4}\tau_3\right) \\ &\quad\cdot x\left(t+\frac{3}{4}\tau_3-\frac{1}{4}\tau_1-\frac{1}{4}\tau_2\right)\cdot e^{-j2\pi f(\tau_1+\tau_2-\tau_3)}d\tau_1 d\tau_2 d\tau_3 \end{aligned} \tag{9}$$

and the sliced symmetric Wigner trispectrum (SWTs) for $k=3$

$$\begin{aligned}
&SW_{s3x}(t,f)\\
&= W^*_{3x}(t,f_1,f_2,f_3)|_{f_1=f_2=-f_3=f}\\
&= \int_{\tau_1}\int_{\tau_2}\int_{\tau_3} x^*\left(t-\frac{1}{4}\tau_1-\frac{1}{4}\tau_2-\frac{1}{4}\tau_3\right)\\
&\quad\cdot x\left(t+\frac{3}{4}\tau_1-\frac{1}{4}\tau_2-\frac{1}{4}\tau_3\right)\cdot x\left(t+\frac{3}{4}\tau_2-\frac{1}{4}\tau_1-\frac{1}{4}\tau_3\right)\\
&\quad\cdot x^*\left(t+\frac{3}{4}\tau_3-\frac{1}{4}\tau_1-\frac{1}{4}\tau_2\right)\cdot e^{-j2\pi f(\tau_1+\tau_2-\tau_3)}d\tau_1 d\tau_2 d\tau_3
\end{aligned} \tag{10}$$

are particular cases of SWHOS. Due to the symmetry, the discrete calculation of SWTs can be simplified as [25]

$$\begin{aligned}
&SW_{s3x}(n,p)\\
&= \frac{1}{N}\exp\Big(j\frac{\pi}{N}np\Big)\sum_{m1=0}^{N-1}\sum_{m2=0}^{N-1}\sum_{m3=0}^{N-1} x^*(n-m1-m2-m3)\\
&\quad\times x(m1)x(m2)x^*(m3)\exp\left(j\frac{2\pi}{N}p(m1+m2)\right)\\
&= \frac{1}{N}\exp\left(j\frac{\pi}{N}np\right)\sum_{m=0}^{2(N-1)}\left[\sum_{m3=0}^{N-1} x^*(n-m-m3)x^*(m3)\right]\\
&\quad\cdot\left[\sum_{m1=0}^{N-1} x(m1)x(m-m1)\right]\exp\left(j\frac{2\pi}{N}pm\right)\\
&= \frac{1}{N}\exp\left(j\frac{\pi}{N}np\right)\sum_{m=0}^{2(N-1)}[x(n-m)*x(n-m)]^*\\
&\quad\cdot[x(m)*x(m)]\exp\left(j\frac{2\pi}{N}pm\right)\\
&= \frac{1}{N}\exp\left(j\frac{\pi}{N}np\right)\sum_{m=0}^{2(N-1)} cx^*(n-m)cx(m)\exp\left(j\frac{2\pi}{N}pm\right)
\end{aligned} \tag{11}$$

where $n$ and $p$ stand for time and frequency samples, $N$ is the total number of signals, and $cx = x*x = \sum_{m=0}^{N-1} x(m)x(n-m)$ ($*$ represents convolution). Compared with SWT, the SWTs has a computational complexity similar to WVD, improving the efficiency of computing. In this paper, we consider the SWB and SWTs as the main representations of SWHOS in practical applications.

As seen from these equations, SWTs in common with WVD is a real valued function, while SWB is a complex function with phase information. SWB and SWTs are two-dimensional time–frequency diagrams, similar to WVD, but based on the multilinear definition of higher order time–frequency representations. Using the property of instantaneous higher order moments, SWB and SWTs are able to retain the more relevant information of signal that represents higher concentration in the time–frequency distributions. However, there are serious cross terms in the SWB and SWTs time–frequency spectrum of multicomponent signal. For example, consider a signal $x(t)$ made up of two monocomponent signals $x_1(t)$ and $x_2(t)$, that is, $x(t)=x_1(t)+x_2(t)$. The corresponding SWB is given by

$$\begin{aligned}
SW_{2x}(t,f) = {}& SW_{2x_1}(t,f)+SW_{2x_2}(t,f)\\
&+3SW_{x_1x_1x_2}(t,f)+3SW_{x_1x_2x_2}(t,f)
\end{aligned} \tag{12}$$

where $3SW_{x_1x_1x_2}(t,f)$ and $3SW_{x_1x_2x_2}(t,f)$ are cross terms. These cross terms will lead to false components, undermining the effectiveness of time–frequency spectrum. Similarly, SWTs suffers from cross term issue.

**Algorithm 1:** MP-SWHOS.

Inputs: $x(t)$ and $N$;
Initialization: $n=0$, $R^0\{x(t)\}=x(t)$;
1: While $n \le N-1$
2: MP process: calculate atom
$g_{\gamma_n}(t) = \arg\max_{g_\gamma\in D}|\langle R^n\{x(t)\}, g_\gamma(t)\rangle|$
and corresponding amplitude
$a_n = |\langle R^n\{x(t)\}, g_{\gamma_n}(t)\rangle|$;
3: calculate atom's $SW_{2g_{\gamma_n}}(t,f)$and $SW_{s3g_{\gamma_n}}(t,f)$;
4: $R^{n+1}\{x(t)\} = R^n\{x(t)\} - a_n g_{\gamma_n}(t)$;
5: $n=n+1$;
6: End while
7: calculate MP-SWHOS

$$\mathrm{MP-SWB}(t,f) = \sum_{n=0}^{N-1} {a_n}^2 SW_{2g_{\gamma_n}}(t,f)$$

$$\mathrm{MP-SWTs}(t,f) = \sum_{n=0}^{N-1} {a_n}^2 SW_{s3g_{\gamma_n}}(t,f)$$

Outputs: $\mathrm{MP-SWB}(t,f)$ and $\mathrm{MP-SWTs}(t,f)$.

### *C. Matching Pursuit-Based Sliced Wigner Higher Order Spectra*

In this paper, we combine MP and SWHOS to propose MP-SWHOS, which can avoid cross term interference. According to (4), the MP-SWHOS of signal $x(t)$ can be typically given by MP-SWB and MP-SWTs ($k=2,3$)

$$\mathrm{MP-SWB}(t,f) = \sum_{n=0}^{N-1} {a_n}^2 SW_{2g_{\gamma_n}}(t,f) \tag{13}$$

$$\mathrm{MP-SWTs}(t,f) = \sum_{n=0}^{N-1} {a_n}^2 SW_{s3g_{\gamma_n}}(t,f). \tag{14}$$

In (13) and (14), the SWHOS of residual $R^N\{x(t)\}$, considered as noise interference, are ignored. The MP-SWHOS are able to characterize the MP time–frequency spectrum as MP-WVD, but with different preference information. The energy distribution of signal is given by MP-WVD, while MP-SWHOS express higher order correlation representation varying with time and frequency. In addition, a higher order local correlation for monocomponent will lead to a sparser representation in time–frequency spectrum. Considering the advantages of MP and SWHOS, MP-SWB and MP-SWTs are able to obtain the sparser and higher concentrated time–frequency distributions without cross terms. Algorithm 1 gives the summary of

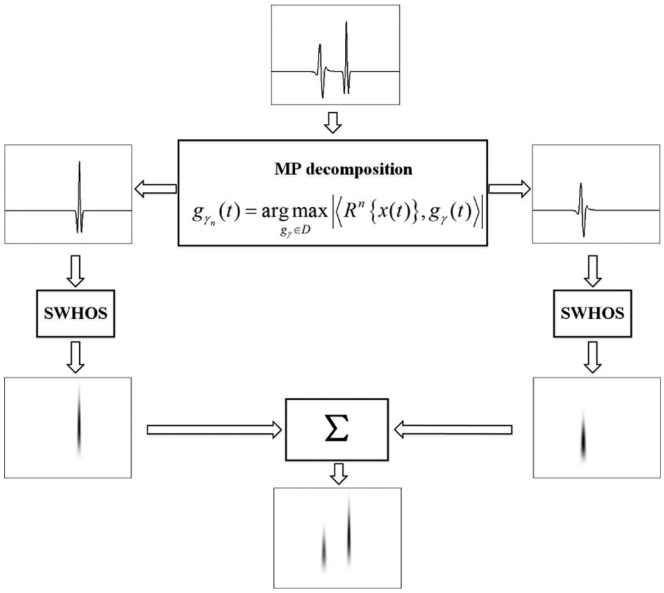


Fig. 1. An overview of MP-SWHOS. For a multicomponent signal, first use MP algorithm, decompose it into several atoms, then calculate the SWHOS of every atom, and finally sum over these SWHOS results ($\sum$ represents a summation process).

TABLE I
PARAMETERS OF WAVELETS R1–R5

| Wavelets | $u$ | $f$ | $\varphi$ | Amplitude |
|---|---|---|---|---|
| R1 | 0.2 | 20 | 0 | 0.5 |
| R2 | 0.4 | 45 | $\pi/4$ | 0.8 |
| R3 | 0.6 | 35 | $\pi/2$ | 0.7 |
| R4 | 0.79 | 55 | 0 | 1 |
| R5 | 0.81 | 55 | 0 | $-1$ |

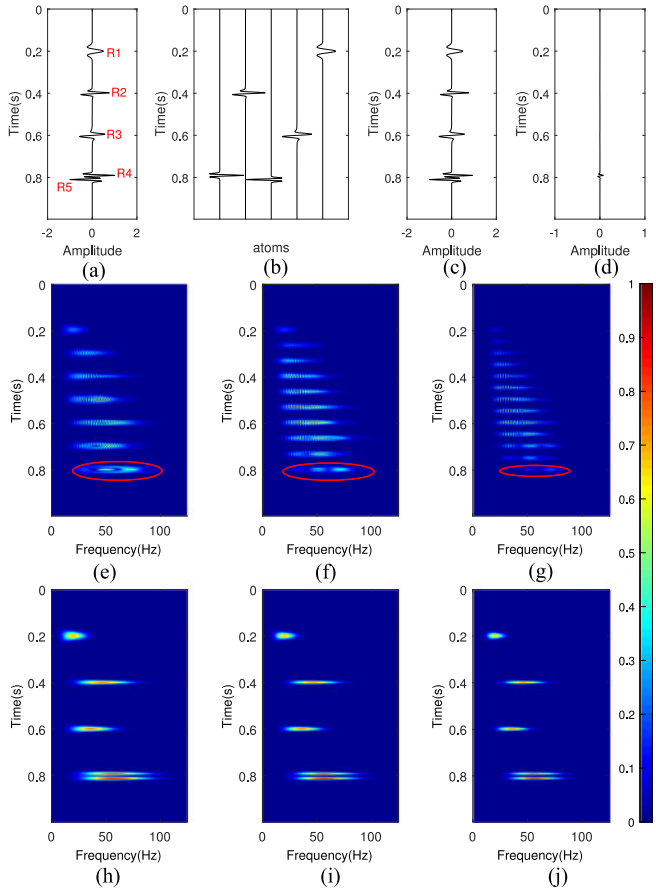


Fig. 2. Simulated model and its time–frequency distributions. (a) Simulated model; (b) MP decomposition results after five iterations; (c) reconstructed signal; (d) residual; (e) WVD; (f) SWB; (g) SWTs; (h) MP-WVD; (i) MP-SWB; (j) MP-SWTs.

MP-SWHOS algorithm, and an overview of MP-SWHOS is outlined in Fig. 1.

## III. EXPERIMENTS AND ANALYSIS

All experiments in this paper are based on MATLAB with the higher-order spectral analysis toolbox. For better comparison, the maximum value of the time–frequency spectrum has been normalized.

### A. Simulated Model

In the first experiment, we consider a simulated model without noise as shown in Fig. 2(a). The simulated model has a total of 500 points and is composed of five constant-phase Ricker wavelets R1–R5 with the parameters given in Table I. It may be noted that wavelets R4 and R5 have partial overlap. In addition, Fig. 2(b)–(d) shows the five atoms of MP decomposition results after five iterations, the reconstructed signal and residual. As seen from these figures, several atoms which closely fit the structures of simulated model are obtained by the MP algorithm, and the residual after five iterations [Fig. 2(d)] is so small that it can be neglected. The comparison of different time–frequency distributions is represented by Fig. 2(e)–(j). There are serious cross term phenomena in the time–frequency distributions of WVD, SWB, and SWTs [Fig. 2(e)–(g)]. In particular in the red ellipses, the wavelets R4 and R5 interfere. However, MP-WVD, MP-SWB, and MP-SWTs [Fig. 2(h)–(j)] effectively eliminate cross terms. The wavelets R4 and R5 can be clearly distinguished from each other in these distributions.

A criterion for the distribution-concentration is defined as [30]

$$M = \frac{\int_{-\infty}^{\infty}\int_{-\infty}^{\infty} |P(t,f)|^4 dtdf}{\left(\int_{-\infty}^{\infty}\int_{-\infty}^{\infty} |P(t,f)|^2 dtdf\right)^2} \tag{15}$$

where $P(t,f)$ represents time–frequency distribution. This quantitative evaluation is similar to equivalent measures of kurtosis, peakedness, or sharpness. The distribution that has a larger $M$ is better concentrated. Moreover, the norm $L_0$ represents the number of nonzero elements; thus, $L_0/K$ can be used to evaluate the sparsity of the entire distribution where $K$ stands for the total number of matrix elements. A smaller $L_0/K$ implies a sparser result. These two criteria are calculated to compare the performance of distributions. Table II lists the $M$, $L_0$, $L_0/K$ values and average time cost over 100 runs (second) of the distributions in Fig. 2(e)–(j). Due to cross terms, the WVD,

TABLE II
$M$, $L_0$, $L_0/K$ VALUES AND AVERAGE TIME COST (OVER 100 RUNS) OF FIG. 2(E)–(J) DISTRIBUTIONS

| Distributions | $M$ | $L_0$ | $L_0/K$ | Time cost (s) |
|---|---|---|---|---|
| WVD | 0.1333 | 34 725 | 0.1389 | 0.0185 |
| SWB | 0.1383 | 51 069 | 0.2043 | 2.0543 |
| SWTs | 0.1646 | 49 392 | 0.1976 | 0.0814 |
| MP-WVD | 0.1427 | 10 526 | 0.0421 | 0.0966 |
| MP-SWB | 0.1553 | 7767 | 0.0311 | 10.1310 |
| MP-SWTs | 0.1752 | 5317 | 0.0213 | 0.4364 |

TABLE III
$M$, $L_0$, $L_0/K$ VALUES AND AVERAGE TIME COST (OVER 100 RUNS) OF FIG. 3(E)– (J) DISTRIBUTIONS

| Distributions | $M$ | $L_0$ | $L_0/K$ | Time cost (s) |
|---|---|---|---|---|
| WVD | 0.1027 | 238 621 | 0.9545 | 0.0200 |
| SWB | 0.1095 | 246 423 | 0.9857 | 2.1741 |
| SWTs | 0.1350 | 242 262 | 0.9690 | 0.0835 |
| MP-WVD | 0.1536 | 9825 | 0.0393 | 0.1106 |
| MP-SWB | 0.1709 | 6775 | 0.0271 | 10.1027 |
| MP-SWTs | 0.1887 | 4518 | 0.0181 | 0.4575 |

SWB, and SWTs have smaller $M$ and larger $L_0$, $L_0/K$ values than the corresponding MP-based distribution. This implies that the MP-based algorithms improve the performance of concentration and sparsity. It is evident that the MP-SWB and MP-SWTs have better time–frequency concentration and higher sparsity compared to MP-WVD. In addition, MP-SWB and MP-SWTs have more time cost than MP-WVD, but MP-SWTs is faster than MP-SWB.

The second experiment with our method is carried out on the simulated model with additive white Gaussian noise, giving a signal-to-noise ratio of 5 dB. The noisy model and its MP decomposition results after five iterations are shown in Fig. 3(a) and (b), displaying the corresponding reconstructed signal and residual in Fig. 3(c) and (d). As seen from these figures, five atoms are well separated from the noisy model, and noise is retained as residual [Fig. 3(d)]. Fig. 3(e)– (j) shows the time–frequency distributions of noisy model. It is obvious that WVD, SWB, and SWTs suffer from cross term issues and noise interference [Fig. 3(e)–(g)]. In contrast, these matters are removed in the time–frequency distributions of MP-WVD, MP-SWB, and MP-SWT [Fig. 3(h)–(j)]. A comparison of the distribution performance of these methods is displayed in Table III. From these data, it is obvious that the WVD, SWB, and SWTs are easily influenced by noise, resulting in large deviations from no-noise results (Table II). However, these deviations do not appear in the results of MP-WVD, MP-SWB, and MP-SWTs. They still work well for noisy signal. Furthermore, the time–frequency concentrations and sparsity of MP-SWB and MP-SWTs are superior to that of MP-WVD. For synthetic models, its quality of reconstruction can be evaluated by

$$Q = 10\log_{10}\frac{\|x(t)-\hat{x}(t)\|_2^2}{\|\hat{x}(t)\|_2^2} \tag{16}$$

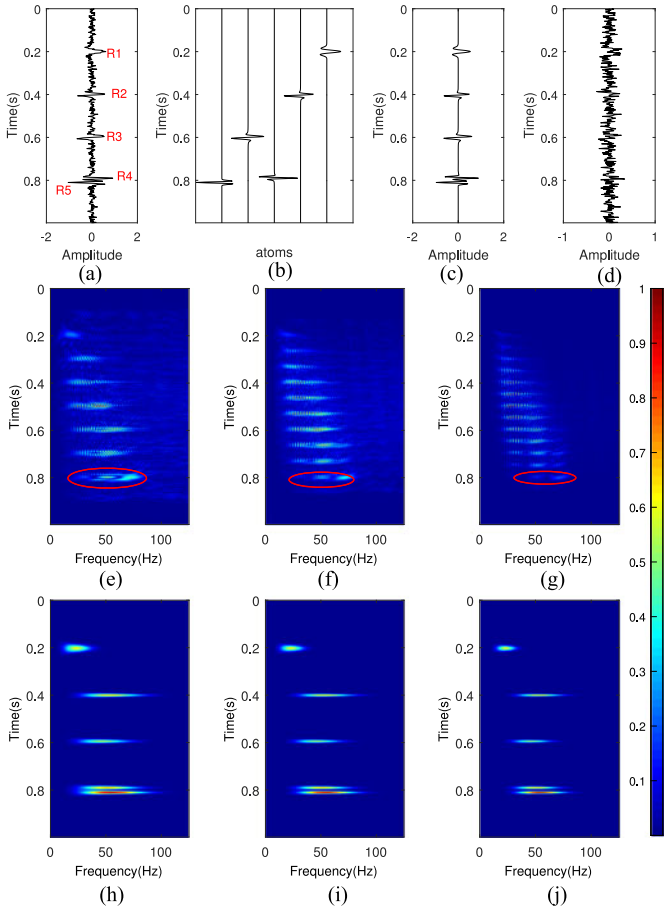


Fig. 3. Noisy model and its time–frequency distributions. (a) Noisy model; (b) MP decomposition results after five iterations; (c) reconstructed signal; (d) residual; (e) WVD; (f) SWB; (g) SWTs; (h) MP-WVD; (i) MP-SWB; (j) MP-SWTs.

where $x(t)$ is the true signal and $\hat{x}(t)$ is the reconstructed signal. The quantitative evaluation $Q$ value varies with iteration $N$, which is plotted in Fig. 4(a). Due to the effect of noise interference, the noisy result is always larger than the no-noise result. With the iteration number increasing, the $Q$ value becomes smaller and the reconstructed signal is getting closer to the true signal. And $Q$ can reach a relatively small value at five iterations. In addition, we also give the computational time curve of MP-WVD, MP-SWB, and MP-SWTs with respect to iteration $N$ in Fig. 4(b). Under the same iteration number $N$, the computational time of MP-SWB is two orders of magnitude larger than that of MP-WVD. In contrast, MP-SWTs demands a time cost closer to MP-WVD. The robustness of MP-SWB and MP-SWTs is verified by the noisy model testing. These simulation tests indicate that the MP-SWHOS can improve the time–frequency concentration and sparsity of MP-WVD, and perform well even in a noisy situation.

### *B. Real Seismic Data*

A real seismic signal given in Fig. 5(a) is used to test the performance of MP-SWHOS algorithm. The different time–frequency distributions of the real seismic signal are clearly

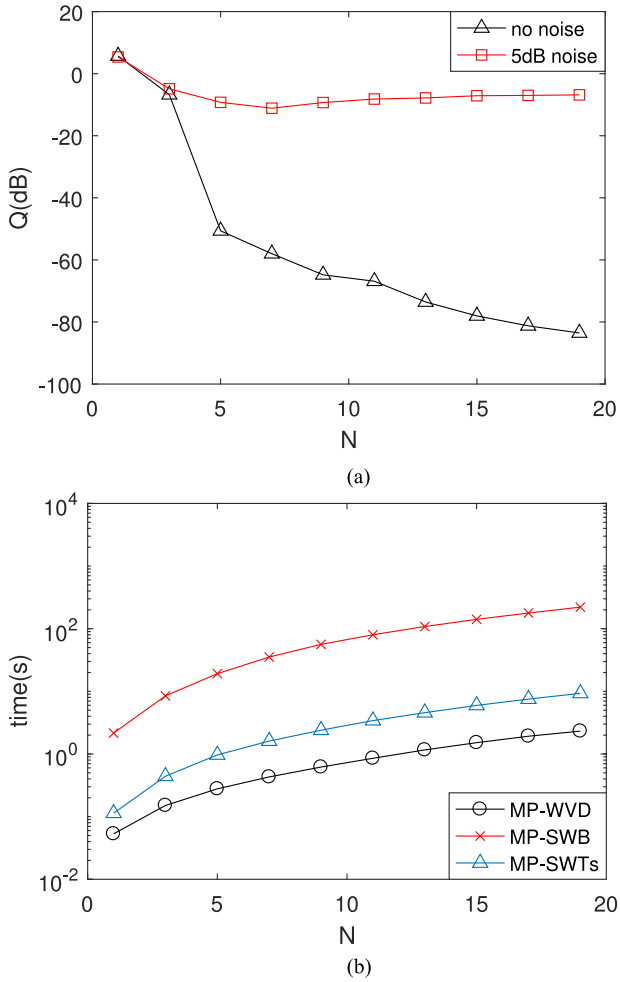


Fig. 4. Performance evaluation (a) $Q$ value evaluation curve with iteration $N$; (b) computational time curve with iteration $N$ by means of MP-WVD, MP-SWB, and MP-SWTs.

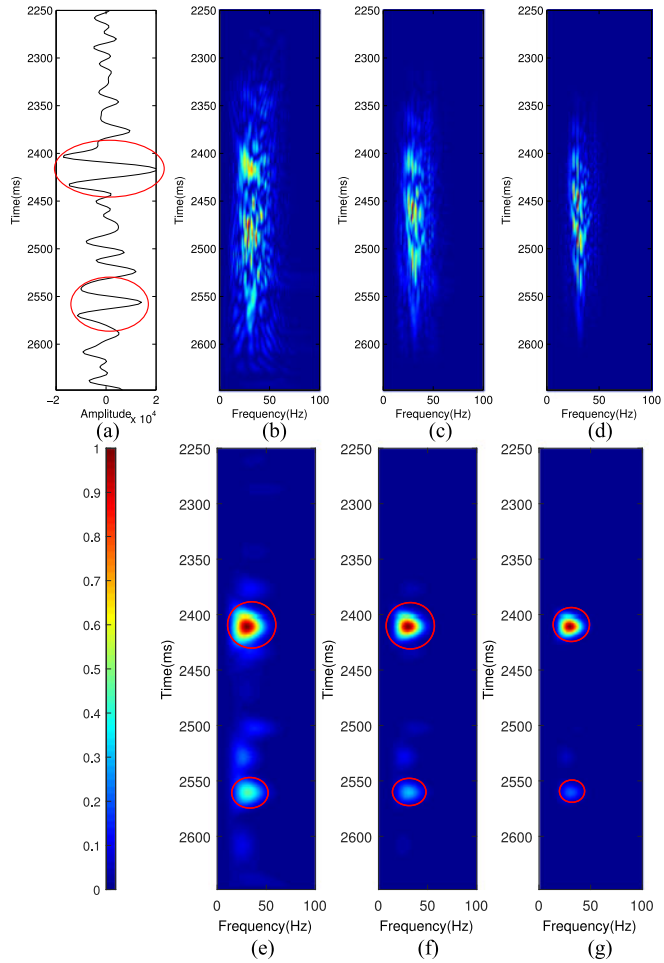


Fig. 5. A real seismic signal and its time–frequency distributions. (a) A real seismic signal; (b) WVD; (c) SWB; (d) SWTs; (e) MP-WVD with 20 iterations; (f) MP-SWB with 20 iterations; (g) MP-SWTs with 20 iterations.

TABLE IV
$M$, $L_0$, $L_0/K$ VALUES AND AVERAGE TIME COST (OVER 100 RUNS) OF FIG. 5(B)– (G) DISTRIBUTIONS

| Distributions | $M$ | $L_0$ | $L_0/K$ | Time cost (s) |
|---|---|---|---|---|
| WVD | 0.1422 | 23 415 | 0.0893 | 0.0047 |
| SWB | 0.1519 | 18 407 | 0.0702 | 0.2042 |
| SWTs | 0.1820 | 8222 | 0.0314 | 0.0174 |
| MP-WVD | 0.1540 | 20 557 | 0.0784 | 0.0850 |
| MP-SWB | 0.1960 | 10 474 | 0.0400 | 4.1870 |
| MP-SWTs | 0.2313 | 5488 | 0.0209 | 0.2795 |

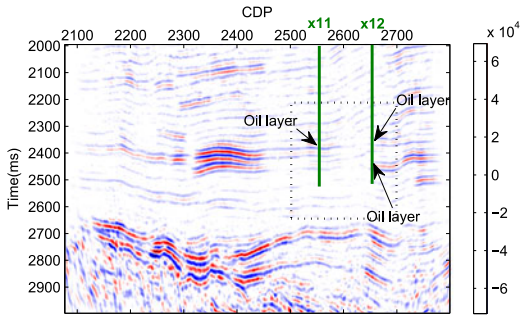


Fig. 6. A partial seismic profile from the Lixian Slope of Bohai Bay Basin.

visible in Fig. 5(b)–(g) with a performance summarized in Table IV. The signal has two obvious components at around 2420 ms and 2560 ms [red circles in Fig. 5(a)]. For Fig. 5(b)– (d), it is difficult to distinguish the main components of the real seismic signal. The WVD, SWB, and SWTs perform poorly for seismic signal due to the cross term disturbance. This limitation is solved by MP-WVD, MP-SWB, and MP-SWTs. As shown in Fig. 5(e)– (g), these distributions well characterize the two components of the real seismic signal without cross terms. It is obvious that the MP-SWB and MP-SWTs are better concentrated and sparser than MP-WVD. The MP-SWHOS with a higher order can produce a better localized time–frequency distribution.

Now we apply the MP-SWHOS method to a real seismic data example with target carbonate oil reservoirs. As shown in Fig. 6, a seismic section is derived from the Lixian Slope of Bohai Bay Basin with two wells denoted $\times 11$ and $\times 12$ (green

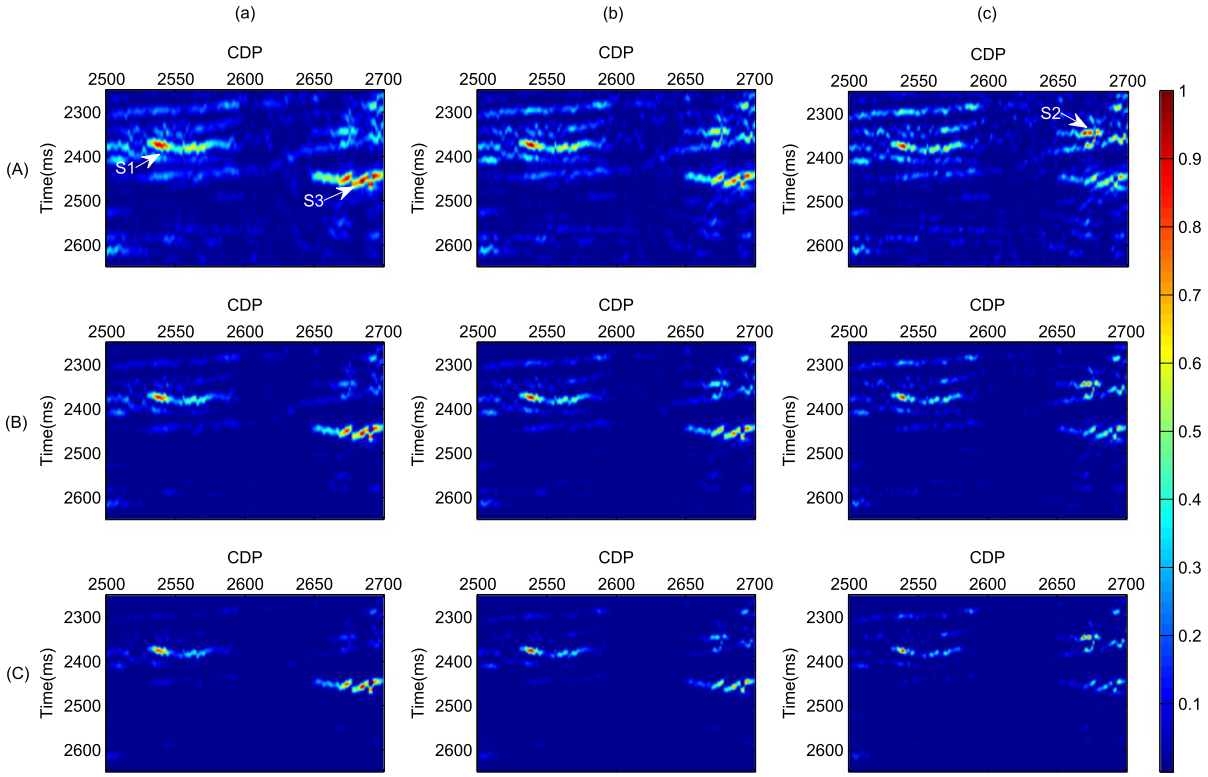


Fig. 7. Spectral decomposition results. (a) 15 Hz slices, (b) 25 Hz slices, and (c) 35 Hz slices. (A) results of MP-WVD, (B) results of MP-SWB, and (C) results of MP-SWTs.

lines). Logging data indicate that there are three oil reservoirs located at 2350 ms, 2380 ms, and 2450 ms, respectively. We delineate a dashed rectangle area, where the window time is 2250–2648 ms and the common depth point range is 2500–2700. This region contains 201 seismic traces with the sampling interval of 2 ms. The spectral decomposition results of dashed rectangle area can be used to interpret seismic data in the single-frequency domain. Fig. 7 shows the 30 Hz, 40 Hz, and 50 Hz single-frequency slices extracted by MP-WVD, MP-SWB, and MP-SWTs. These maps indicate the changes of three significant energy groups at S1, S2, and S3, which are consistent with the actual reservoir location. The energy appearing at S1 and S2 becomes stronger in the higher frequency slices, while there is an obvious energy attenuation at S3. However, these changes are more easily observed in the results of MP-SWB and MP-SWTs [Fig. 7(B) and (C)] due to the effect of resolution.

Through comparison in these figures, the spectral decomposition results of MP-SWB and MP-SWTs are better localized than those of MP-WVD, and have clear energy attenuation in accord with the actual reservoir information. Compared with MP-SWB, MP-SWTs does not increase the computational cost while improving the resolution. The spectral decomposition results of MP-SWHOS are clearly suitable for seismic analysis, enhancing the interpretation of potential hydrocarbon reservoirs. The real seismic data application demonstrates that MP-SWHOS are effective for seismic spectral decomposition, and can improve the time–frequency concentration and sparsity of MP-WVD.

## IV. Conclusion

In this paper, we presented a new time–frequency method termed the MP-SWHOS by using the SWHOS instead of WVD to obtain the MP time–frequency spectrum. This approach is based on the theory of MP-WVD and SWHOS. By using the MP algorithm, the cross term issue of SWHOS can be removed. Rather than calculating a WVD, we are able to improve spectral resolution by adopting SWHOS.

Both simulated and real seismic data were tested to demonstrate that MP-SWHOS possess superior energy resolution and sparsity in comparison with MP-WVD. Using MP-SWHOS, we can obtain the high-precision spectral decomposition results of seismic signal. Furthermore, MP-SWTs can provide a better concentrated and sparser distribution with higher computational efficiency than MP-SWB. In the field data processing, MP-SWTs is a better choice for spectral decomposition among MP-SWHOS.

## References

[1] P. Flandrin and P. Borgnat, "Time-frequency energy distributions meet compressed sensing," *IEEE Trans. Signal Process.*, vol. 58, no. 6, pp. 2974–2982, Jun. 2010.

[2] X. Wu and T. Liu, "Spectral decomposition of seismic data with reassigned smoothed pseudo Wigner–Ville distribution," *J. Appl. Geophys.*, vol. 68, no. 3, pp. 386–393, Jul. 2009.

[3] R. B. Pachori and A. Nishad, "Cross-terms reduction in the Wigner–Ville distribution using tunable-Q wavelet transform," *Signal Process.*, vol. 120, pp. 288–304, Mar. 2016.

[4] R. B. Pachori and P. Sircar, "A new technique to reduce cross terms in the Wigner distribution," *Digital Signal Process.*, vol. 17, no. 2, pp. 466–474, Mar. 2007.
[5] N. A. Khan and M. Sandsten, "Time–frequency image enhancement based on interference suppression in Wigner–Ville distribution," *Signal Process.*, vol. 127, pp. 80–85, Oct. 2016.
[6] I. Zoukaneri and M. J. Porsani, "A combined Wigner–Ville and maximum entropy method for high-resolution time-frequency analysis of seismic data," *Geophysics*, vol. 80, no. 6, pp. O1–O11, Nov. 2015.
[7] L. Tian and Z. Peng, "Determining the optimal order of fractional Gabor transform based on kurtosis maximization and its application," *J. Appl. Geophys.*, vol. 108, pp. 152–158, Sep. 2014.
[8] Y. Wang, Z. Peng, and Y. He, "Instantaneous attributes analysis of seismic signals using improved HHT," *J. Earth Sci.*, vol. 26, no. 4, pp. 515–521, Aug. 2015.
[9] Y. Wang and Z. Peng, "The optimal fractional s transform of seismic signal based on the normalized second-order central moment," *J. Appl. Geophys.*, vol. 129, pp. 8–16, Jun. 2016.
[10] Z.-l. Huang, J. Zhang, T.-h. Zhao, and Y. Sun, "Synchrosqueezing S-transform and its application in seismic spectral decomposition," *IEEE Trans. Geosci. Remote Sens.*, vol. 54, no. 2, pp. 817–825, Feb. 2016.
[11] K. H. Miah and D. K. Potter, "Geophysical signal parameterization and filtering using the fractional Fourier transform," *IEEE J. Sel. Topics Appl. Earth Observ. Remote Sens.*, vol. 7, no. 3, pp. 845–852, Sep. 2014.
[12] B. Wang, "An amplitude preserving s-transform for seismic data attenuation compensation," *IEEE Signal Process. Lett.*, vol. 23, no. 9, pp. 1155–1159, Mar. 2016.
[13] S. G. Mallat and Z. Zhang, "Matching pursuits with time-frequency dictionaries," *IEEE Trans. Signal Process.*, vol. 41, no. 12, pp. 3397–3415, Dec. 1993.
[14] K. Schiecke, M. Wacker, F. Benninger, M. Feucht, L. Leistritz, and H. Witte, "Matching pursuit based time-variant bispectral analysis and its application to biomedical signals," *IEEE Trans. Biomed. Eng.*, vol. 62, no. 8, pp. 1937–1947, Aug. 2015.
[15] G. Li and R. J. Burkholder, "Hybrid matching pursuit for distributed through-wall radar imaging," *IEEE Trans. Antennas Propag.*, vol. 63, no. 4, pp. 1701–1711, Apr. 2015.
[16] G. Li, H. Zhang, X. Wang, and X. Xia, "Isar 2-D imaging of uniformly rotating targets via matching pursuit," *IEEE Trans. Aerosp. Electron. Syst.*, vol. 48, no. 2, pp. 1838–1846, Apr. 2012.
[17] A. Chakraborty and D. Okaya, "Frequency-time decomposition of seismic data using wavelet-based methods," *Geophysics*, vol. 60, no. 6, pp. 1906–1916, Apr. 1995.
[18] J. Liu, Y. Wu, D. Han, X. Li et al.,"Time-frequency decomposition based on ricker wavelet," in *Proc. 74th Annu. Meeting Soc. Explor. Geophys.*, Denver, CO, USA, Oct. 2004, pp. 1937–1940.
[19] J. Liu *et al.*, "Matching pursuit decomposition using morlet wavelets," in *Proc. 75th Annu. Meeting Soc. Explor. Geophys.*, Houston, TX, USA, Nov. 2005, pp. 786–789.
[20] Y. Wang, "Seismic time-frequency spectral decomposition by matching pursuit," *Geophysics*, vol. 72, no. 1, pp. V13–V20, Jan. 2006.
[21] T. Zhao and W. Song, "An application of matching pursuit time-frequency decomposition method using multi-wavelet dictionaries," *Petrol. Sci.*, vol. 9, no. 3, pp. 310–316, Sep. 2012.
[22] H. Lin, Y. Li, H. Ma, B. Yang, and J. Dai, "Matching-pursuit-based spatial-trace time-frequency peak filtering for seismic random noise attenuation," *IEEE Geosci. Remote Sens. Lett.*, vol. 12, no. 2, pp. 394–398, Feb. 2015.
[23] J. R. Fonollosa and C. L. Nikias, "Analysis of transient signals using higher-order time-frequency distributions," in *Proc. IEEE Int. Conf. Acoust. Speech Signal Process.*, vol. 5, 1992, pp. 197–200.
[24] J. R. Fonoliosa and C. Nikias, "Wigner higher order moment spectra: Definition, properties, computation and application to transient signal analysis," *IEEE Trans. Signal Process.*, vol. 41, no. 1, pp. 245–266, Jan. 1993.
[25] J. R. Fonollosa and C. L. Nikias, "Analysis of finite-energy signals higher-order moments-and spectra-based time-frequency distributions," *Signal Process.*, vol. 36, no. 3, pp. 315–328, Apr. 1994.
[26] Q. Guo, H. Yu, J. Hu, and A. Xu, "Transient fault signal detection using Wigner higher-order moment spectra methods," in *Proc. 2006 IEEE Int. Conf. Mechatronics Autom.*, Jun. 2006, pp. 2421–2425.
[27] L. Luo, Y. Xu, and J. Yuan, "Identification of flow regime transitions in an annulus sparged internal loop airlift reactor based on higher order statistics and Winger trispectrum," *Chem. Eng. Sci.*, vol. 66, no. 21, pp. 5224–5235, Nov. 2011.
[28] L. Gelman, I. Petrunin, and J. Komoda, "The new chirp-Wigner higher order spectra for transient signals with any known nonlinear frequency variation," *Mech. Syst. Signal Process.*, vol. 24, no. 2, pp. 567–571, Feb. 2010.
[29] S. Levy and D. Oldenburg, "Automatic phase correction of common-midpoint stacked data," *Geophysics*, vol. 52, no. 1, pp. 51–59, Jan. 1987.
[30] D. L. Jones and T. W. Parks, "A high resolution data-adaptive time-frequency representation," *IEEE Trans. Acoust., Speech, Signal Process.*, vol. 38, no. 12, pp. 2127–2135, Dec. 1990.

**Yuqing Wang** received the Bachelor's degree from the University of Electronic Science and Technology of China (UESTC), Chengdu, Sichuan, China, in 2013. She is currently working toward the Ph.D. degree in the field of seismic time–frequency analysis and attribute extraction at School of Optoelectronic Information, UESTC.

Her research interests include signal processing, time–frequency analysis, seismic attribute analysis, and fluid identification.

**Zhenming Peng** (M'06) received the Ph.D. degree in geo-detection and information technology from Chengdu University of Technology, Chengdu, China, in 2001. From 2001 to 2003, he was a Postdoctoral Researcher with the Institute of Optics and Electronics, Chinese Academy of Sciences, Chengdu, China.

He is currently a professor with University of Electronic Science and Technology, Chengdu, China. His research interests include image processing, radar signal processing, and target recognition and tracking.

Prof. Peng is a member of the Aerospace Society of China.

**Xiaoyang Wang** received the B.S. degree in electronic science and technology from the University of Electronic Science and Technology of China (UESTC), Chengdu, China, in 2013. She is currently working toward Ph.D. degree in computer vision at UESTC.

Her research interests include image processing, infrared target detection, and object tracking.

**Yanmin He** received the Ph.D. degree in the School of Automation Engineering, University of Electronic Science and Technology of China (UESTC), Chengdu, China, in 2011.

She is currently an Assistant Professor with the School of Optoelectronic Information, UESTC. She has published more than 20 peer-reviewed papers, and she is the inventor or coinventor of ten patents. Her research interests include signal processing and pattern recognition.